Degradation of structure and properties of rail surface layer at long-term operation

Materials Science and Technology, http://dx.doi.org/10.1080/02670836.2017.1287983 (2017)

Degradation of structure and properties of rail surface layer at long-term operation

V.E. Gromov[1,*], Yu.F. Ivanov[2,3], R. S. Qin[4], O.A. Peregudov[1], K.V. Aksenova[1], O.A. Semina[1]

[1] Siberian State Industrial University, 654007 Novokuznetsk, Russia

[2] Institute of High-Current Electronics of the Siberian Branch of the Russian Academy of Science, 634055 Tomsk, Russia

[3] National Research Tomsk Polytechnic University, 634050 Tomsk, Russia

[4]School of Engineering & Innovation, The Open University, Milton Keynes MK7 6AA, UK

Abstract: The microstructure evolution and properties variation of the surface layer of rail steel after passed 500 and 1000 million tons of gross weight (MTGW) have been investigated. The wear rate increases to 3 and 3.4 times after passed 500 and 1000 MTGW, respectively. The corresponding friction coefficient decreases by 1.4 and 1.1 times. The cementite plates were destroyed and formed the cementite particles of around 10-50 nm in size after passed 500 MTGW. The early stage dynamical recrystallization was observed after passed 1000 MTGW. The mechanisms for these have been suggested. The large number of bend extinction contours is revealed in the surface layer. The internal stress field is evaluated.

Keywords: Rail steel; Microstructure; Defect substructure; Internal stress.

* Corresponding author. E-mail address: gromov@physics.sibsiu.ru ; Tel. +7 3843 462277

Introduction

The increasing volume of freight, improving speed of train and simultaneous growing loading accelerate the wear of tread surface and failure of rails.[1-4] Wear is the main factor responsible for the rails traffic capacity and service life.[3,4] Up to 15% of all rails have impermissible wear or crumpling norms, which have been removed as single withdrawal. This problem has attracted considerable interests from researchers in materials science and physical metallurgy. After a comparatively short term operation, i.e. having supported the transportation of 100-500 million tons of gross weight (hereafter named MTGW), one can observe severe plastic deformations and microstructure transformation.[5-12] These include the bended and fractured cementite plates, high dislocation density around interface, dissolved cementite and formed austenite. A white layer with microhardness around 12 GPa forms on the rail surface. Cementite is very stable in normal conditions. The deformation-induced failure of cementite indicates a shift of phase balance, which affects the performance of rails afterwards. The surface layers of rails possess abnormally high value of microhardness and consist bimodal distribution of grain sizes in the range of 20–500 nm. At high stress level a ferrite matrix behaves similar to viscoelastic liquid [13].There are significant efforts devoted to the analysis of structure and composition transformations of rails in long-term operation.[14-21]

The aim of the present work was to analyze the transformation of structure and properties of rail surface layer after long-term operation in railways.

Experiments

R65 rail steel was studied in the present work. The steel has a chemical composition in weight percentage of C: 0.75; Mn: 0.85; Si: 0.40; Cr: 0.42; N: 0.12; Cu: 0.14; V: 0.12; Al: < 0.015; P: <0.02; S: < 0.02. Samples were cut from the rail before service and also after long term

operational service (passed 500 MTGW and 1000 MTGW). The investigation focuses on the surface layer of rail tread contact zone. The samples were studied by metallographic method (i.e. transverse etched metallographic sections using 4% alcoholic solution of nitric acid for etching), scanning and transmission diffraction electron microscopes.[16,17] Thin foils were prepared by electrolytic thinning of same plates, which were cut by electro-spark method directly from the surface layer of tread contact zone of rail head [22, 23]. Fig. 1 illustrated the sample location in a rail steel.

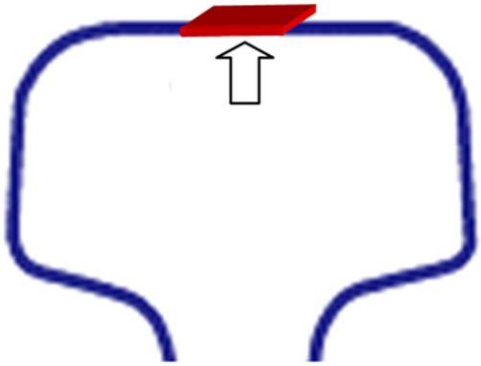

Figure 1. Schematic diagram shows the samples position (where an arrow is pointing to) in rail steel.

The Vickers hardness of the steel surface layer was measured (PMT-3). More than 50 indents were used to obtain the average hardness. The grains size was determined using the casual secant method which across over more than 50 grains for the the calculation of average grain size.[1] The wear resistance was examined using a tribometer (Tribotechnic, made in France). A ball of 3 mm diameter taken from the quenched steel was used as counterbody. Measurements were made according to the scheme of sample rotation in stationary counterbody. The linear rate of rotation was 2.0-2.5 cm/s. The rated load on counterbody was 10 N. The number of sample rotation was 5000. The measurements for the profile of friction groove on the sample surface with numerical determination of friction groove depth and its cross-section area were

done after completion of friction process by tribometer. Wear resistance was assessed by the inverse value to wear rate or intensity of wear. Wear rate was calculated according to the following formula

$$V = \frac{2 \cdot \pi \cdot R \cdot A}{F \cdot L} \quad (1)$$

where R is the radius of track (mm). A is cross-section area of wear groove (mm^2). F is the applied load (N) and L the distance travelled by counterbody ball (m). Scalar dislocation density in grains of different morphology was measured by casual secant method.[22]

Results and Discussion

Visual examination of un-etched metallographic sections reveals a smooth bright line that indicates a long-term operation after passed 500 MTGW and 1000 MTGW. The tribological test shows the reduction of wear resistance after long term operation. The rail's wear resistance decreases by around 3 times after passing 500 MTGW and by 3.4 times after 1000 MTGW. The decrease of wear resistance is accompanied with the reduction of friction coefficient. The change of friction coefficient is smaller as the increase of the operating loan.

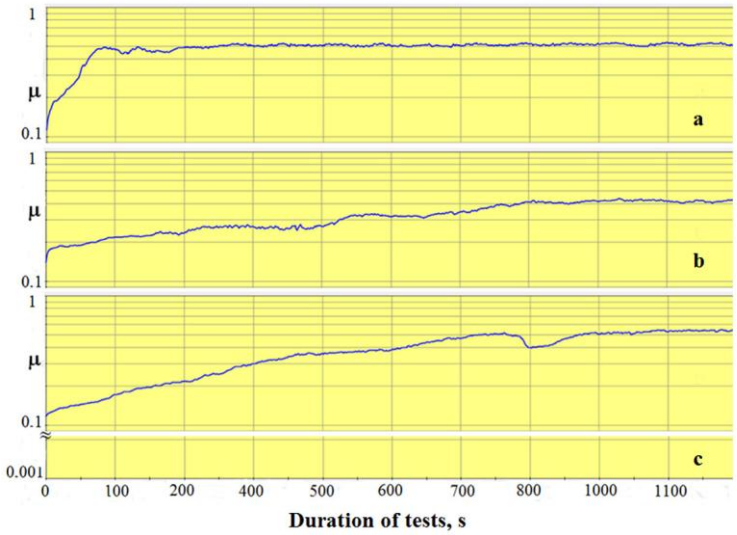

Figure 2. The change of friction coefficient μ for (a) new steel, (b) steel after 500 MTGW loading, and (c) steel after 1000 MTGW loading. The wear resistance tests were done on rail tread surface.

The changes of friction coefficient for various steel samples are presented in Fig. 2. The curves can be separated into two stages: the initial stage (stage of running-in) with variable friction coefficient and the basic stage with rather stable friction coefficient. For the steel samples taken from new rail without any operating loading, the initial stage is less than 100 s, as shown in Fig. 2(a). The sample taken from 500 MTGW rail shows an initial stage in 800 s, as shown in Fig. 2(b). The sample taken from 1000 MTGW rail has an initial stage around 1000 s, as shown in Fig. 2(c).

The evolution of tribological properties of the samples is accompanied with a change in hardness at its surface layer. Vickers hardness were measured with a load of 2 N. The surface layer of new rail has a hardness of 5.7 GPa. It increased to 7.0 GPa for the steel after 500 MTGW but reduced to 5.4 GPa for the steel after 1000 MTGW.

It is suggested that the change in hardness and tribological properties in operation is due to the change of microstructure and composition on the surface layer of the steels. Along the site of severe plastic deformation on the surface, the thickness of the white region of work-hardened metal is up to 30 μm. The area away from the surface shows insignificant dispersion of pearlite and reduction of ferrite fraction. The grain size in steel is independent of distance to the tread surface.

The transmission electron microscope (TEM) image for the new steel sample is presented in Fig. 3. It contains lamellar pearlite, mixture of ferrite and carbide grains, and structure-free ferrite grains. The dislocations with a scalar density 10^{10} cm^{-2} are distributed randomly in the structure-free ferrite. In pearlite, dislocations with a scalar density of 4×10^{10} cm^{-2} are distributed as a net-like substructure. The scalar dislocation density reaches a maximum value

of 8×10^{10} cm^{-2} near the globular carbide particles. The pearlite is a eutectoid mixture of ferrite and cementite plates. The lamellar pearlite shows various imperfections: e.g. ferrite bridges (ferrite is divided by the cementite plate), curved cementite plates, unparalleled and aggregated structure. The dark field analysis shows the substructure of cementite where cementite plates are divided into fragments of 30-50 nm in size.

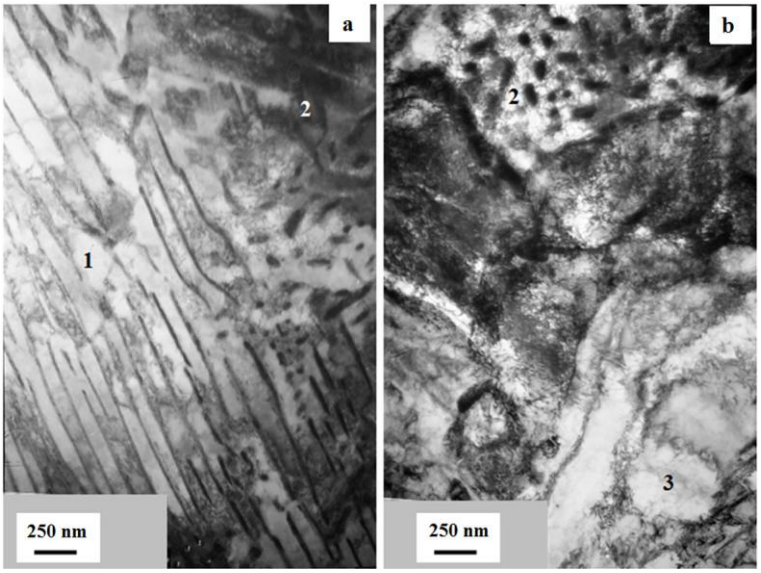

Figure 3. TEM image of new rail steel, where 1 labels the pearlite, 2 ferrite and carbide grains mixture, and 3 structure-free ferrite grains

The microstructure in the surface layer of rail materials changes significantly after 500 MTGW, as shown in Fig. 4. Cementite plates in pearlite colonies are fractured completely. Some globular cementite particles with size in 30-50 nm and 10-15 nm are discovered, see in Fig. 4(a) and 4(b), respectively. It is suggested that the 30-50 nm particles are formed due to the destruction of cementite plates, and the 10-15 nm particles are formed due to the decomposition of the supersaturated solid solution under severe plastic deformation. The fragmentation of cementite is also witnessed by the observation of 150 nm fragments. Substructures can be noticed inside the fragments. The scalar dislocation density in the substructure reaches 10^{11} cm^{-2}, as shown in Fig. 4(a).

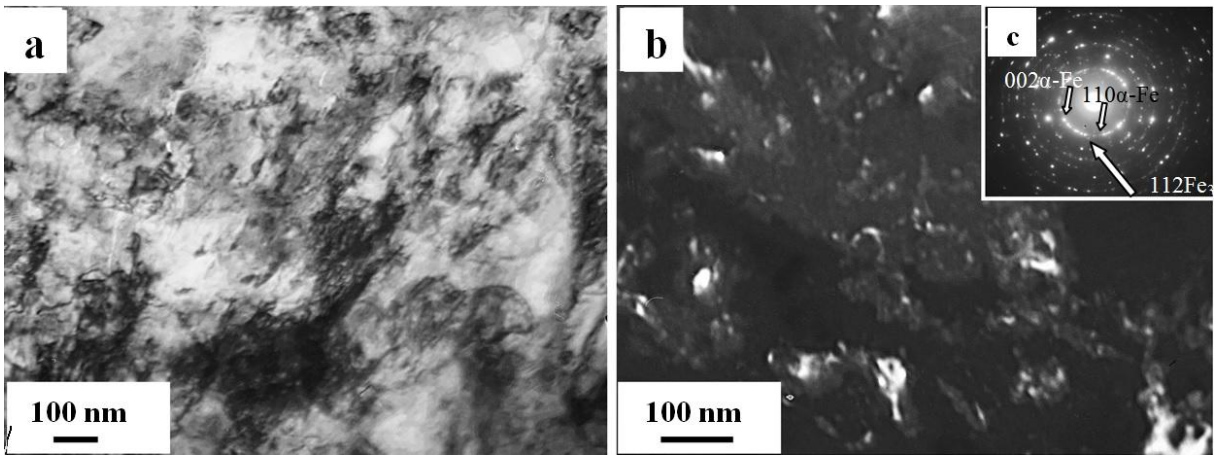

Figure 4. TEM images reveal the microstructure in surface layer of rail steel after 500 MTGW loading. (a) light field; (b) dark field obtained in reflection [112] Fe_3C; (c) micro-electron diffraction pattern, arrow designates the reflection in which dark field was obtained.

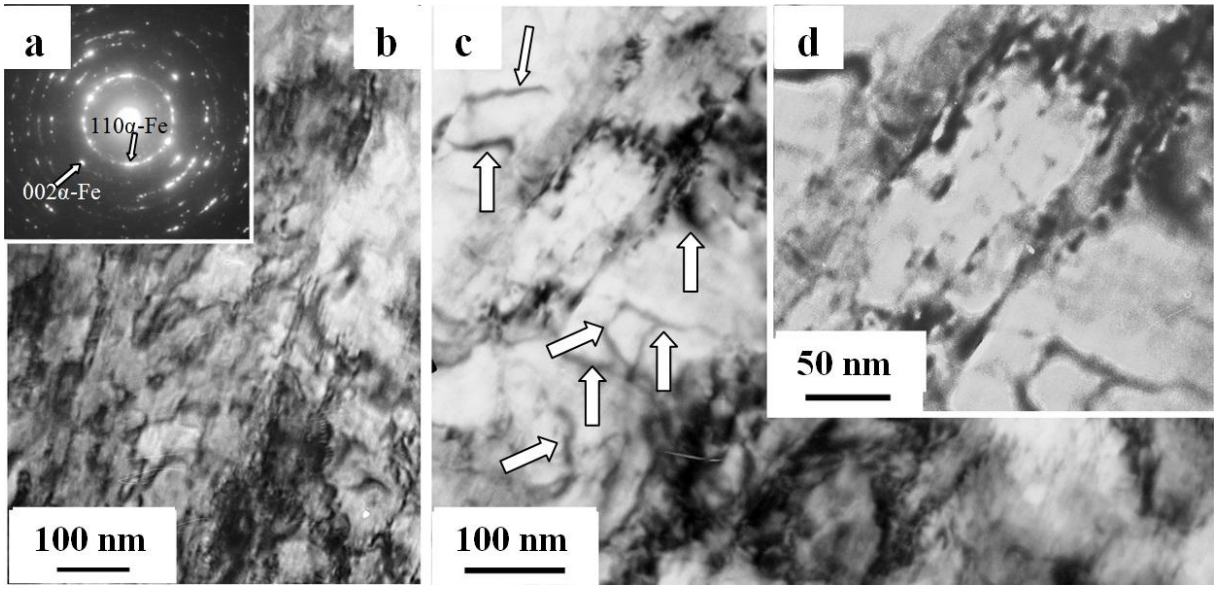

Figure 5. SEM and TEM image for the surface layer of steel after 500 MTGW loading. (a) diffraction patter from (b); (b)-(d) are the light field images.

The service of rail steel is accompanied by transformation of defects in structure-free ferrite grains. Band substructures are observed in Fig. 5. The distance between bands is 20-30 nm. Around the band structure boundaries one can see the carbide particles whose sizes vary between 5 to 7 nm, as shown in Fig. 5(d). This indicates the presence of two competitive

processes during loading service, namely (1) the fragmentation of cementite as well as ferrite grain and plates and (2) the dissolution of cementite particles, transition of carbon atoms into dislocations (in Cottrell atmospheres), transportation of carbon atoms by dislocations into ferrite grains or plates followed by repeated formation of nano dimensional particles of cementite. This causes the formation of nanocrystalline multiphase structure in the surface layer of steel after 500 MTGW. The hardness of the steel increases by a factor of 1.2 approximately.

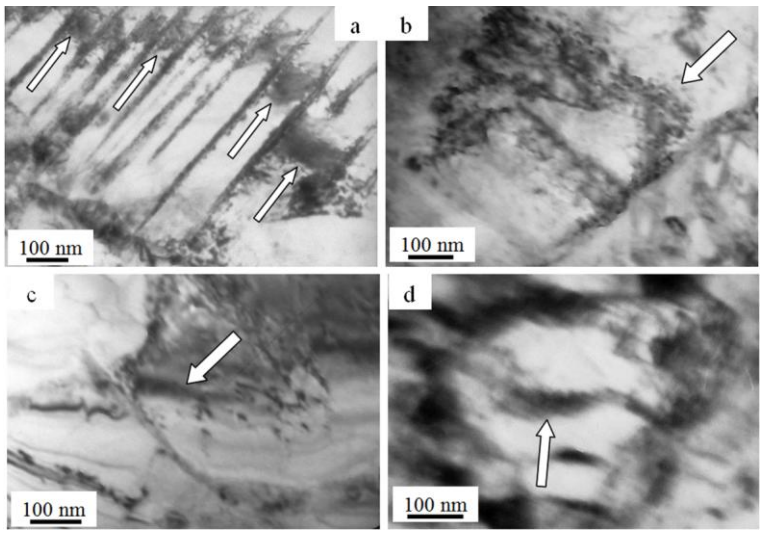

Figure 6. TEM images show the internal stress bend extinction contours.

The surface layer shows is a large number of bend extinction contours, as shown in Fig. 6(a). This provides evidence for the existence of internal stress fields. It can be seen that the stress is concentrated at the interfaces of cementite plates in pearlite, and the interface between pearlite grains and ferrite grains, as shown in Fig. 6(b). In the latter case the stress extinction contour initiates from the interface of plate and/or grains. Stress fields are often arising from the precipitates and secondary phases located at the interface and also inside the grains, as shown in Fig. 6(c) and 6(d).

The bending of materials crystal lattice may cause elastic deformation initially. The stress is accumulated due to incompatibility of deformation in polycrystalline[24] and non-deformable

inclusions.[11] The source of stress fields of elastic origin is initiated in the junctions and boundaries of polycrystalline grains under uniform deformation, around the disperse non-deformable particles, or near cracks.[25] Later on the bending may be created by dislocation and become plastic due to excess localized dislocation density in the material. The bending can also be elastic-plastic when both sources are present in the material.

The estimation of internal stress profile along the corresponding extinction contours requires determining the lattice curvature-torsion. For this purpose either the displacement rate of extinction contour under changes of goniometer slope angle or the width of extinction contour should be measured.[1,26] It has been established that with simultaneous use of both procedures the width of extinction contour in values of disorientations in hardened steels was around 1 degree.[26] The amplitude of curvature-torsion χ is determined by the value of continuous disorientation gradient

$$\chi = \frac{\partial \varphi}{\partial \ell}, \tag{2}$$

where $\partial\varphi$ is the change of orientation reflecting the planes of foils, and $\partial\ell$ is the value of displacement of extinction contour. Testing assessments carried out on hardened steels as well as steels subjected to different degrees and types of deformation showed that reasonable assessments of value of internal stress fields could be done using the following relationship [1]

$$\sigma_\tau = Gt\frac{\partial \varphi}{\partial \ell} \approx 10^{-2} G\frac{t}{h}, \tag{3}$$

where *h* is transverse size of bend extinction contour (≈ 5 – 200 nm), *t* the width of foil (It is corresponded to 200 nm[22,23]) and *G* the shear modulus of steel (80 GPa). Therefore, the morphology of bend extinction contours characterizes the gradient of curvature-torsion of

material crystal lattice, the value of transverse size of contours – the amplitude of curvature-torsion of crystal lattice.

The capacity of bend extinction contour (internal stress fields generated by this contour) is characterized by its transverse size – the less are the transverse sizes of contour the higher is amplitude of internal stress fields.[1,22] Using this character it can be noted that the stress fields of maximum amplitude are formed by interface particle/matrix, as shown is Fig. 6(c) and 6(d). These values exceed the tensile strength of rails (i.e. ~1.2 GPa).

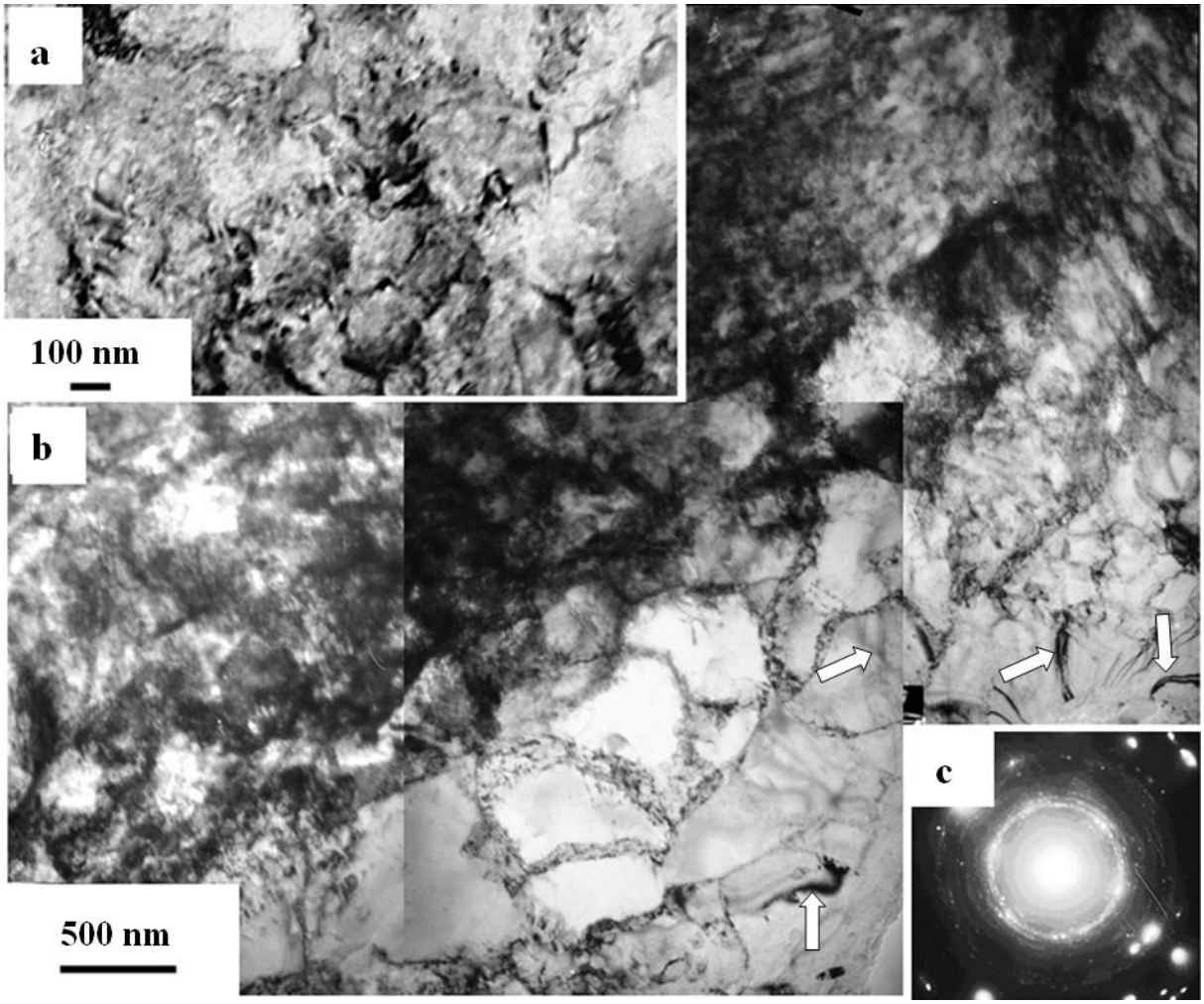

Figure 7. Electron microscope image for surface layer of the rail steel after 1000 MTGW: (a) and (b) are in light fields; (c) is the micro-electron diffraction pattern.

Significant differences in structure-phase state of the material were revealed in rail steels after 1000 MTGW over that of 500 MTGW. Firstly, the defect substructure in ferrite grains differs essentially. It was shown in Fig. 5 that a band structure was formed inside the ferrite grains after 500 MTGW. After 1000 MTGW a predominantly sub-grain structure is revealed in ferrite grains. This indicates the proceeding the initial stage of dynamic recrystallization, as shown in Fig. 7(b). Inside the sub-grains chaotically located dislocations are discovered. The scalar density of the dislocations is less than 10^8 cm^{-2}. Another difference is a formation of structure in the surfaces layer. Fig. 7(c) is the micro-electron diffraction patterns obtained from the microstructure shown in Fig. 7(a). The pattern contains separately located point reflections that belong to α-phase (solid solution based on bcc iron) and a large number of thin diffraction rings that belong, most likely, to nanoscale particles of carbide and oxy-carbide phases. One can suppose that failure in colonies of lamellar pearlite and dynamic recrystallization of ferrite grains can facilitate the reduction in hardness of steel surface layer up to the value of hardness of initial state. In Fig.5 and Fig.7 the extinction contours are designated by the arrows. If we compare the extinction contours and band structure boundaries, it is seen that the contours are diffused and have a diverse shape (very curved). The band substructures boundaries have a dislocation origin, i.e. they are formed from dislocations

Conclusion

The reduction of wear resistance at rail tread surface after operation at railway and passed 500 MTGW and 1000 MTGW was revealed. It was shown that a highly effective nanoscale crystalline multiphase structure was formed in the surface layer of rail after passed 500 MTGW. This contributes to the increment of in steel hardness by 1.2 times. When the 1000

MTGW were passed on the steel, pearlite grains collapsed and a dynamic recrystallization was initialized, which caused the softening of rail surface layer.

After long-term operation, density of bend extinction contours is increased at the surface layer of rail steel. This indicates the formation of internal stress field. A quantitative analysis reveals that the stress fields are mainly located at the interfaces between carbides particle and matrix.

Acknowledgments

The work was sponsored financially by the Russian Science Foundation under project №15-12-00010.

References

1. V.E. Gromov, A.B. Yuriev, K.V. Morozov, Yu.F. Ivanov, Microstructure of hardened rails, Cambridge, CISP, 2015.
2. V.I. Vorozhishchev The composition and production technology of the rails increased efficiency, Novokuznetsk, Izd-vo “Novokuznetskii poligraficheskii kombinat”, 2008.
3. E.A. Shur, Damage to the rails, Moscow, Intekst, 2012.
4. E. Sheinman, J. Friction Wear, 2012, **33**, 308-314.
5. Yu. Ivanisenko, H.J. Fecht, Steel Tech., 2008, **3**, 19–23.
6. Yu. Ivanisenko, I. Maclaren, X. Sauvage, R.Z. Valiev, H.-J. Fecht, Acta Mater., 2006, **54**, 1659–1669.
7. J. L. Ning, E. Courtois-Manara, I. Kurmanaeva, A.V. Ganeev, R.Z. Valiev, C. Kübel, Yu. Ivanisenko, Mater. Sci. Eng. A, 2013, **581**, 8–15.
8. V.G. Gavriljuk, Mater. Sci. Eng. A, 2013, **345**, 81–89.

9. Y.J. Li, P. Chai, C. Bochers, S. Westerkamp, S. Goto, D. Raabe, R. Kirchheim, Acta Mater., 2011, **59**, 3965–3977.
10. V.G. Gavriljuk, Scripta Mater., 2001, **45**, 1469–1472.
11. V.V. Rybin, Large plastic deformation and fracture of metals, Moscow, Metallurgiya, 1986.
12. V.E. Gromov, V.A. Petrunin, Physica Status Solidi (a), 1993, **139**, 77-84.
13. Yu. Ivanisenko, W. Lojkowski, and H. J. Fecht, Mater. Sci. Forum, 2007, **539–543**, 4681-4686
14. Yu. Ivanisenko, R.K.Wunderlich, R.Z. Valiev, H.-J. Fecht, Scripta Materialia, 2003, **49**, 947-952.
15. I. MacLaren, Yu. Ivanisenko, H.-J.Fecht, X.Sauvage,, R.Z. Valiev, Ultrafine Grained Materials IV. Ed. By Zhu E.T. et al. The Minerals, Metals & Materials Society, 2006, 1-616.
16. K.S. Kumar, H.Swygenhoven, S. Van, Suresh Acta Materialia, 2003, **51**, 5743-5774.
17. Yu. Ivanisenko, W. Lojkowski, R.Z.Valiev, H.-J. Fecht, Acta Mater., 2003, **51**, 5555-5570.
18. M.A. Meyers, A.Mishra, D.J. Benson, Progress in Materials Science, 2006. 51. 427-556
19. Yu.F. Ivanov, V.E. Gromov, O.A. Peregudov, K.V. Morozov, A.B. Yuriev, Steel in translation, 2015, **45**, 254-257.
20. V.E. Gromov, O.A. Peregudov, Yu.F. Ivanov, K.V. Morozov, K.V. Alsaraeva, O.A. Semina, J. of Surf. Inv. X-ray, Synchr. and Neutr. Techn., 2016, **10**, 76–82.
21. Peregudov, V. E. Gromov, Yu. F. Ivanov, K.V. Morozov, K.V. Alsaraeva, O.A. Semina, AIP Conference Proceedings, 2015, **1683**, 020179.
22. P.B. Hirsch, A. Howie, R.B. Nicholson, D.W. Pashley, M.J. Whelan, Electron microscopy of thin crystals, Melbourne, Krieger Publishing Co., 1977.

23. L.M. Utevskii, The diffraction electron microscopy in physical metallurgy, Moscow, Metallurgiya, 1973.
23. V.E. Panin, V.A. Likhachev, Y. Grinyaev, Structural levels of deformation of solids, Novosibirsk, Nauka, 1985.
24. J. Eshelby, The continuum theory of dislocations, Moscow, ILI, 1963.
25. V.E. Gromov, E.V. Kozlov, V.I. Bazaikin et al., Physics and Mechanics of Drawing and Die Forging, Moscow, Nedra. 1997.